UNIVERSITY OF LEEDS

This is a repository copy of *Comparison of PI and PR Controllers with Adaptive Notch Filter for LCL Filtered Grid-Tie Converters under Weak Grid*.

White Rose Research Online URL for this paper:
http://eprints.whiterose.ac.uk/157019/

Version: Accepted Version

Proceedings Paper:
Rufa'I, NA, Zhang, L and Chong, B (2019) Comparison of PI and PR Controllers with Adaptive Notch Filter for LCL Filtered Grid-Tie Converters under Weak Grid. In: Proceedings of 2019 IEEE PES/IAS PowerAfrica. 2019 IEEE PES/IAS PowerAfrica, 20-23 Aug 2019, Abuja, Nigeria. IEEE , pp. 650-655. ISBN 978-1-7281-1010-3

https://doi.org/10.1109/PowerAfrica.2019.8928912

© 2019 IEEE. This is an author produced version of a paper published in Proceedings of 2019 IEEE PES/IAS PowerAfrica. Personal use of this material is permitted. Permission from IEEE must be obtained for all other uses, in any current or future media, including reprinting/republishing this material for advertising or promotional purposes, creating new collective works, for resale or redistribution to servers or lists, or reuse of any copyrighted component of this work in other works. Uploaded in accordance with the publisher's self-archiving policy.

Reuse
Items deposited in White Rose Research Online are protected by copyright, with all rights reserved unless indicated otherwise. They may be downloaded and/or printed for private study, or other acts as permitted by national copyright laws. The publisher or other rights holders may allow further reproduction and re-use of the full text version. This is indicated by the licence information on the White Rose Research Online record for the item.

Takedown
If you consider content in White Rose Research Online to be in breach of UK law, please notify us by emailing eprints@whiterose.ac.uk including the URL of the record and the reason for the withdrawal request.

White Rose university consortium
Universities of Leeds, Sheffield & York

eprints@whiterose.ac.uk
https://eprints.whiterose.ac.uk/

Comparison of PI and PR Controllers with Adaptive Notch Filter for LCL Filtered Grid-Tie Converters under Weak Grid

Nabila Ahmed Rufa'I, Member, IEEE, Li Zhang and Benjamin Chong
School of Electronic and Electrical Engineering
University of Leeds
Leeds, United Kingdom
el12nari@leeds.ac.uk

Abstract—Renewable energy sources such as solar and wind require power converters and harmonic filters for interconnection with the grid. Central to the operation of such systems is the controller, which ensures that the maximum possible power is transferred from the source to the grid. Of these controllers, the proportional-integral (PI) controller is the most commonly used, owing to its ease of implementation. This report therefore aims at comparing the operation of the PI controller with its stationary reference frame equivalent known as the proportional-resonant (PR) controller. Both controllers are implemented in the voltage oriented control scheme for a three phase converter connected to a weak grid through an LCL filter. The characteristics of the controllers are analysed and compared in both the time and frequency domains. Simulation results validate the performance of each controller.

Index Terms—PI controller; PR controller; adaptive notch filter; weak grid

I. INTRODUCTION

Voltage source converters (VSC) with LCL- type filters are efficient and cost-effective devices to interface the distributed generators connected on a DC-bus with the AC grid. To maintain balanced power exchange between both sides, a VSC requires an effective current control scheme. The most commonly used controller is the PI controller [1, 2], owing to its ease of parameter tuning and implementation. However, the major problems associated with this particular controller include: inaccuracies in tracking a sinusoidal reference signal and reduced periodic disturbance rejection capability [3].

To overcome these limitations, the PI controller is implemented using a dq0- frame rotating synchronously at grid voltage frequency and oriented such that the d- axis is aligned to the grid voltage vector, V_d. The transformations of the fundamental current components into this dq0- frame give rise to DC quantities, hence enabling the PI controller in tracking non-periodic DC reference signals. In addition, to improve its dynamic tracking and disturbance rejecting performance, a grid voltage feedforward is included in the control loop. However, this may lead to system instability [3].

PR controllers are a special case of PI controllers that can alleviate the aforementioned disadvantages. They are implemented in the stationary reference frame, without voltage feedforward, resulting in a reduced computational burden on the control system. The principle of such a controller is that it causes an infinite gain at a particular resonant frequency, allowing for elimination of steady state errors at that frequency [4]. This makes it possible for the PR controller to accurately track a sinusoidal reference.

This paper compares the performance of the aforementioned controllers for AC grid current control of a grid connected VSC. The grid current harmonic content is suppressed with an LCL filter prior to injection into a weak grid. As an LCL filter has infinite gain at its resonant frequency, it is cascaded with an adaptive notch filter (ANF) to provide active damping at the resonant frequency. Although LCL filters are known to provide good harmonic suppression in grid connected converters, their resonant effect can affect the stability of the entire closed loop control system. The paper therefore aims at investigating the effect of the interaction between the dynamics of the LCL filter and the control system, with emphasis on comparison between the performance of PI and PR controllers.

II. SYSTEM CONFIGURATION AND TRANSFER FUNCTIONS

Figs. 1 and 2 illustrate the voltage oriented control technique [5] implemented for a 3-phase grid connected photovoltaic (PV) system with PI and PR controllers respectively. The grid is modelled as a Thevenin equivalent voltage, V_g in series with the grid resistance, R_g and grid inductance, L_g. A weak grid, by definition, is characterised by a high impedance at the network connection point. The PI controller in Fig. 1 requires 3-phase V/I values to be transformed to their equivalent dq quantities using Park's transform which are DC at the steady-state. Compared to the PR controller in Fig. 2 which uses Clarke transformation of AC quantities, not only does this conversion at every sample duration requires extra computational burden, but also necessitates the inclusion of decoupling terms in the control loop, as well as adding feed-forward voltage control [2]. Grid frequency is tracked using the phase locked loop (PLL) method, enabling both power system transformations to be synchronised with the grid. Active and reactive powers can therefore be controlled independently. An LCL filter provides harmonic cancellation due to converter switching. However, at its resonant frequency, the capacitive and inductive impedances cancel out, producing a negligible resistance with an infinite gain. An ANF is positioned in the forward path of the closed loop current control system, introducing a complex conjugate pair of zeros which cancel out the LCL filter resonant poles [6]. ANF tuning is performed using the discrete Fourier transform (DFT) algorithm as implemented in [6]. The DFT filter is applied to the grid side current, i_g from which the band with the highest frequency is identified as the resonant

frequency.

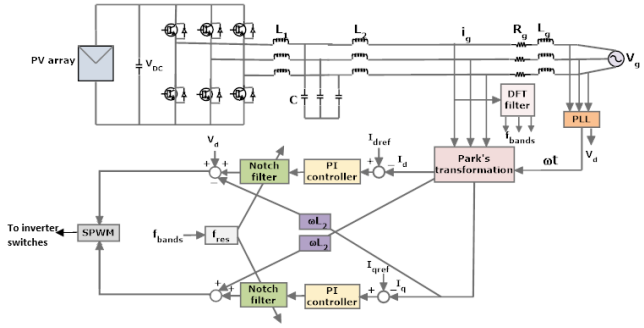

Fig. 1. Voltage oriented control of grid connected VSC with DFT based active damping (PI controller)[6]

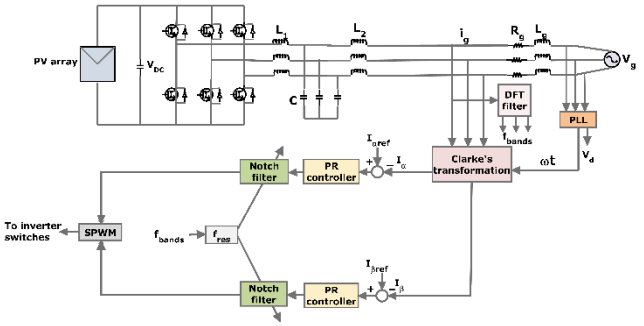

Fig. 2. Voltage oriented control of grid connected VSC with DFT based active damping (PR controller)

The undamped LCL filter transfer function is given by:

$$G_{LCL}(s) = \frac{1}{s^3 L_1 L_2 C + s(L_1 + L_2)}, \quad (1)$$

where L_1, L_2 and C are the filter parameters. The resonant frequency, ω_{res} of the filter is given as:

$$\omega_{res} = \sqrt{\frac{L_1 + (L_2 + L_g)}{L_1 (L_2 + L_g) C}}, \quad (2)$$

where L_g is the inductive component of the grid.

The ANF transfer function is:

$$G_{notch}(s) = \frac{s^2 + 2\zeta_1 \omega_n s + {\omega_n}^2}{s^2 + 2\zeta_2 \omega_n s + {\omega_n}^2}, \quad (3)$$

where ζ_1 is the damping ratio of the NF zeros,

ζ_2 is the damping ratio of the NF poles and

ω_n is the natural frequency of the NF.

As the resonant frequency in (2) varies with the grid inductance, L_g adaptive active damping can only be achieved when ω_{res} is continuously monitored to update ω_n in (3). A DFT filter is therefore applied to monitor the variation and uses the new grid information to retune the NF parameters in (3) [6]. This makes NF adaptive to the grid impedance variation.

The transfer functions for the PI and PR controllers are respectively given as:

$$G_{PI}(s) = K_P + \frac{K_I}{s}, \quad (4)$$

and

$$G_{PR}(s) = K_P + K_I \frac{s}{s^2 + {\omega_o}^2}, \quad (5)$$

where K_P is the proportional gain of the controllers,

K_I is the integral gain of the controllers and

ω_o is the PR controller resonant frequency.

The tuning process for K_I should ensure that it is large enough to eliminate steady state error [7] but not too large as to cause a reduction in phase margin [8]. The controller parameters are tuned using the symmetrical optimum (SO) method, which is a loop shaping design technique [9]. With this method, maximum phase margin is obtained for the entire closed loop system [10, 11]. For simplicity, the higher order LCL filter in (1) may be approximated to a first order L filter, due to the similarity in their characteristics in the low frequency region. The controller parameter ratings are listed in Table I.

Table I: Controller parameter ratings

Parameter	Rating
K_P	10
K_I	5000
ω_o	314.2 rad/s
ω_c	0.5 rad/s

III. Comparisons in Frequency Domain

A. Bode Plot of Controller Transfer Functions

Considering (4), the gain at any arbitrary frequency, ω will be:

$$G_{PI}(j\omega) = K_P + \frac{K_I}{j\omega}. \quad (6)$$

If ω is at 0 rad/s, the transfer function in (6) will have an infinite gain, as:

$$G_{PI}(0) = \infty. \quad (7)$$

The presence of a large gain at 0 rad/s enables the PI controller to track a DC reference without errors, as displayed in the bode plot of Fig. 3.

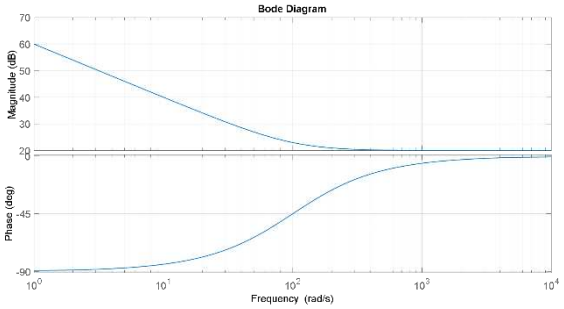

Fig. 3: Open loop Bode plot for PI controllers

Considering (5), the gain at any arbitrary frequency, ω is:

$$G_{PR}(j\omega) = K_P + K_I \frac{s}{-\omega^2 + {\omega_o}^2}. \quad (8)$$

If $\omega = \omega_o$:

$$G_{PR}(j\omega_o) = \infty. \quad (9)$$

From (8) and (9), it is clear that the PR controller offers an infinite gain only at its resonant frequency, ω_o and will not introduce a phase shift at any other frequency [2]. It is therefore capable of tracking periodic signals without errors.

In practice, non-ideal PR controllers with the transfer function in (10) are generally considered, owing to stability issues associated with an infinite gain [12]:

$$G_{PR}(s) = K_P + K_I \frac{2\omega_c s}{s^2+2\omega_c s+{\omega_o}^2}, \quad (10)$$

where ω_c is the bandwidth around the frequency, ω_o.

Fig. 4 shows the ideal and non-ideal PR controller bode plots. K_I sets the width of the band around the resonant frequency [2] and can therefore be narrow in strong grids, where the possibility of frequency variations are minimal.

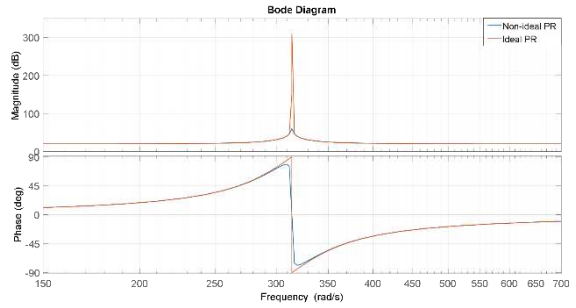

Fig. 4: Open loop Bode plot for PR controllers

B. Bode Plot with a Cascaded Notch Filter

When cascaded with a NF, both controllers respond well as seen in the bode plot of Fig. 5. The PR controller has a large gain at the system frequency of 50 Hz. The responses for both controllers are identical, with the only difference lying in the magnitudes of the low frequency gains prior to the PR resonance frequency. The control system bandwidth frequencies are both 2.67 krad/s with gain margins of 22.5 dB and phase margins of 73.9°. This emphasises that the additional integrator in (5) has no effect on the stability margins of the system. Its core function is to produce a large gain at ω_o for periodic waveform tracking.

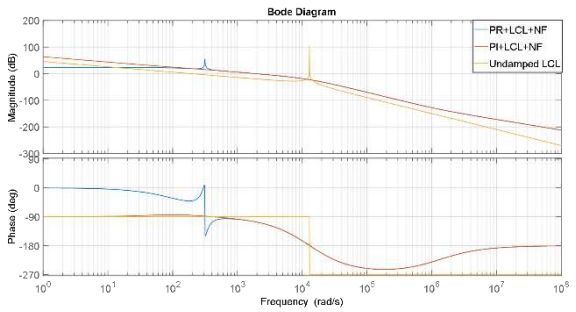

Fig. 5: Open loop Bode plot comparing PI and PR controllers

C. Analysis for a Unit Step Input

If E(s) represents the current feedback error transfer function and R(s) is the input signal transfer function, the steady state error (e_{ss}) for the feedback control system can be computed using the final value theorem (FVT) as:

$$e_{ss} = \lim_{s\to 0} sE(s). \quad (11)$$

Mathematically,

$$E(s) = \frac{1}{1+G_c(s)G(s)} R(s), \quad (12)$$

where G(s) represents the combined transfer function for the PWM delay, LCL filter and grid while $G_c(s)$ is the controller transfer function. The FVT is employed to evaluate the controller response to a step input. For a sinusoidal input, the FVT is not applicable, since no final steady state value exists [13]. The transfer function for a unit step input is:

$$R(s) = \frac{1}{s}. \quad (13)$$

The error signal, E(s) for a PI controller according to (12) is:

$$E(s) = \frac{1}{s+(sK_P+K_I)G(s)}. \quad (14)$$

Applying the final value theorem of (11) to (14):

$$e_{ss} = \lim_{s\to 0} sE(s) = 0. \quad (15)$$

This verifies the ability of a PI controller to eliminate steady state error for a step input, with the aid of the integrator action.

The error signal, E(s) for a PR controller according to (12) is:

$$E(s) = \frac{s^2+{\omega_o}^2}{s^2+{\omega_o}^2+[K_P(s^2+{\omega_o}^2)+K_I]G(s)} \frac{1}{s}. \quad (16)$$

Applying the FVT:

$$e_{ss} = \lim_{s\to 0} sE(s) = \frac{{\omega_o}^2}{{\omega_o}^2+(K_P{\omega_o}^2+K_I]G(s)}. \quad (17)$$

As verified by (17), a steady state error exists for a PR controller tracking a step input.

D. Analysis for a Unit Step Disturbance

For a disturbance, D(s) the transfer function for error due to disturbance, $E_D(s)$ is:

$$E_D(s) = -\frac{G(s)}{1+G_c(s)G(s)} D(s). \quad (18)$$

For a PI controller:

$$E_D(s) = -\frac{sG(s)}{s+(sK_P+K_I)G(s)} D(s). \quad (19)$$

And for a unit step disturbance:

$$E_D(s) = -\frac{G(s)}{s+(sK_P+K_I)G(s)}. \quad (20)$$

Applying the FVT to (20):

$$e_{ss} = \lim_{s\to 0} sE(s) = 0. \quad (21)$$

For a PR controller:

$$E_D(s) = -\frac{G(s)(s^2+{\omega_o}^2)}{s^2+{\omega_o}^2+[K_P(s^2+{\omega_o}^2)+K_I]G(s)} D(s). \quad (22)$$

Applying the FVT to (22):

$$e_{ss} = \lim_{s\to 0} sE(s) = -\frac{{\omega_o}^2 G(s)}{{\omega_o}^2+[K_P{\omega_o}^2+K_I]G(s)}. \quad (23)$$

Equations 21 and 23 verify that while a step disturbance can be rejected by a PI controller, an error persists for a PR controller, since the gain exists only at its resonant frequency.

IV. Comparisons in Control Performance

The performance of the controllers implemented in the current control loops of a grid connected VSC as in Figs. 1 and 2 are investigated with the system parameters specified in

Table II. All simulations are performed using MATLAB/Simulink software.

Table II: System parameter ratings [6]

Parameter	Rating
VSC Rated Power (P)	100 kW
Grid frequency (f)	50 Hz
$L_1/C/L_2$	5 mH/88.4 µF/68.8 µH
Resonant frequency (f_{res})	2.06 kHz (13 krad/s)
Grid Impedance (R_g/ L_g)	0.5 Ω/1 mH
Sampling frequency (f_s)	10 kHz
Notch filter damping ratio (ζ_1/ζ_2)	0.01/1

A. Controller Step Response

The step responses for the controllers are shown in Fig. 6. The rise time for the PR controller is faster by 0.3 ms, which is attributed to the additional integrator. However, as it is tuned to 50 Hz, there is a steady state error of 6.1%, due to the DC input. The PI controller, on the other hand, settles without steady state error.

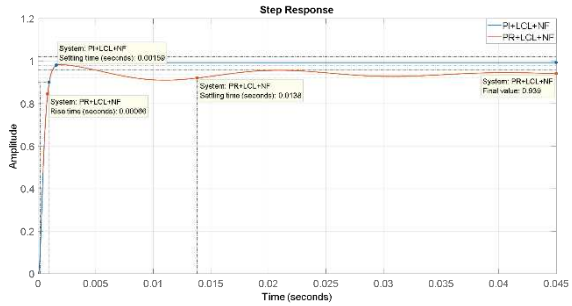

Fig. 6: Comparing step responses for PI and PR controllers

B. AC reference tracking

When provided with a sinusoidal reference, the results for the grid current are seen in Figs. 7 and 8. The PI controller tracks the sinusoidal reference with a visible steady state error, which significantly reduces when the feed forward voltage is considered. To completely eliminate the error, a logical solution is to increase K_I such that a large gain occurs at the reference frequency based on (6). Alternatively, the voltage feedforward term can be increased. Both increments must be carefully implemented as they negatively affect the stability margins of the system, especially in the case of weak grids [14]. The PR controller in Fig. 8, on the other hand, perfectly matches the reference even in the absence of a grid voltage feedforward [2].

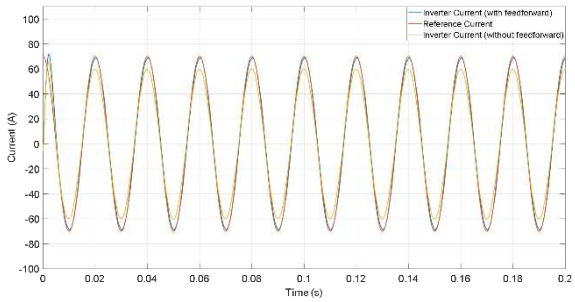

Fig. 7: Grid current with PI Controller tracking an AC reference

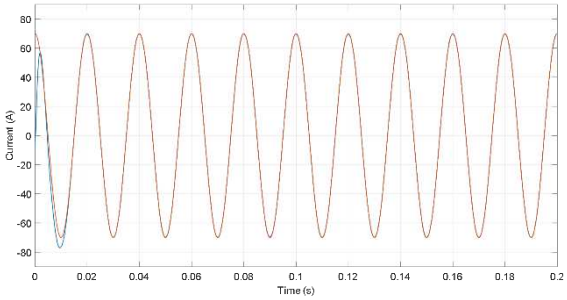

Fig. 8: Grid current with PR Controller tracking an AC reference

C. Disturbance rejection

A disturbance is added to test the robustness of the control systems. The nature of the disturbance itself determines the response of the controller. DC disturbances in the form of asymmetrical faults produce DC offset in electrical power systems [15]. For the DC disturbance introduced in 0.1 seconds as seen in Fig. 9, the PI controller response in Fig. 10 shows the controller is capable of DC disturbance rejection, as proved in (21). The PR control produces an unbalanced current with a DC offset in phase C, as seen in Fig. 11. The phase A current amplitude in the positive half cycle is roughly 10% higher than that of phase C. This further verifies the inability of a PR controller in rejecting DC disturbances, as proved in (23).

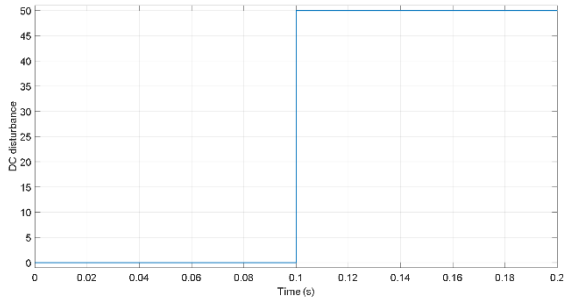

Fig. 9: DC disturbance

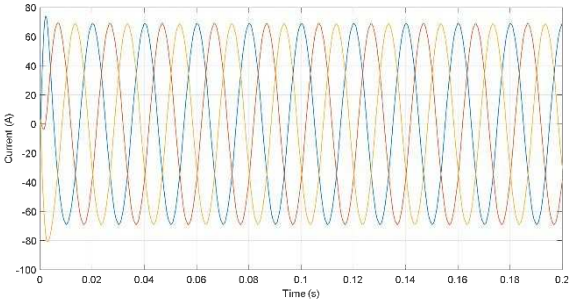

Fig. 10: Grid current with PI controller under a DC disturbance

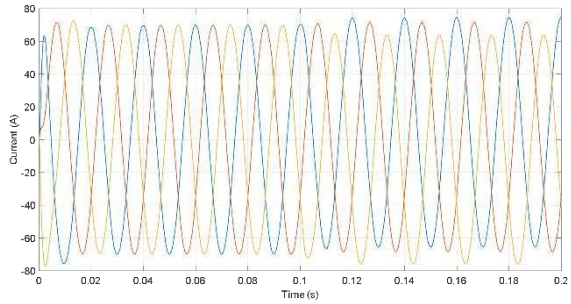

Fig. 11: Grid current with PR controller under a DC disturbance

D. Voltage Harmonics Interference Rejection

For a weak grid consisting of 3rd and 5th order harmonics as seen in Fig. 12, the PI controller produces the current in Fig. 13 with a total harmonic distortion (THD) of 10.86% observed in Fig. 14. The series NF is tuned only to the LCL filter resonance and is therefore incapable of low order harmonic compensation. Furthermore, the PI controller cannot compensate low order harmonics due to its limited bandwidth [2]. Although a higher bandwidth can be achieved by increasing K_P, it will be at the expense of system stability. In the case of the PR controller, the measured grid current in Fig. 15 has a slightly reduced THD value of 7.63% as shown in Fig. 16. Both controllers must therefore be equipped with secondary harmonic compensators (HCs) for adequate grid current harmonic compensation.

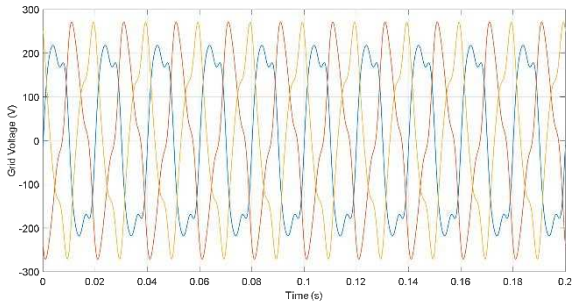

Fig. 12: Grid voltage with 3rd and 5th order harmonics

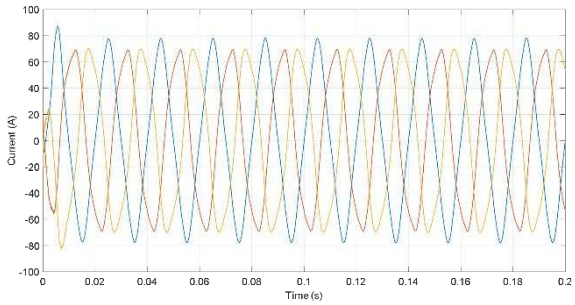

Fig. 13: Grid current with harmonics (PI controller)

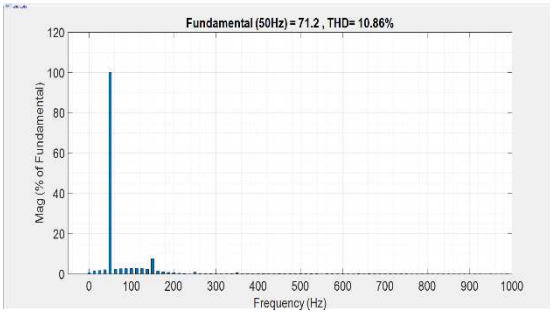

Fig. 14: THD of grid current (PI controller)

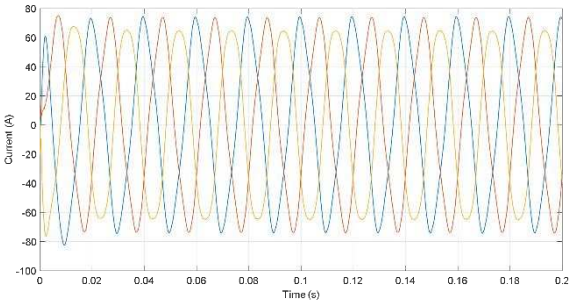

Fig. 15: Grid current with harmonics (PR controller)

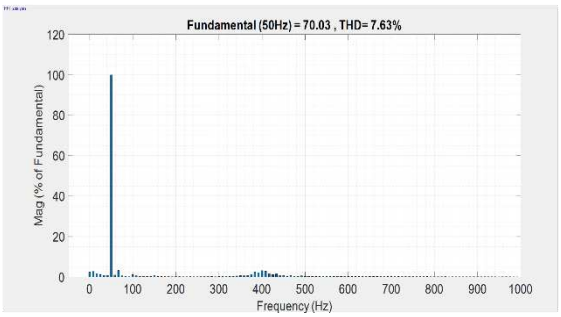

Fig. 16: THD of grid current (PR controller)

The low order harmonics in the PI control system can be compensated through the implementation of a parallel set of HCs in the synchronous reference frame acting on the harmonics in a selective manner. These HCs may also be implemented for the PR control system, as they have no effect on the dynamics of the controller, since they are restricted to frequencies close to their respective resonant frequencies [16]. The ideal HC transfer function for the h^{th} harmonic is given by:

$$G_{HC}(s) = \sum_{h=3,5,7,\ldots} K_{Ih} \frac{s}{s^2+(h\omega_o)^2}. \quad (24)$$

E. Varied grid impedance

When the grid impedance in Figs. 1 and 2 changes from 1 mH to 5 mH, the short circuit ratio (SCR) of the system changes from that of a strong to a weak grid [6, 17]. For a change in grid inductance, L_g the resonant frequency of the LCL filter will also vary according to (2). Figs. 17 and 18 show the grid current responses of both control systems when the NF is initially tuned to the resonant frequency corresponding to 1 mH. For a change in grid inductance to 5 mH, both control systems are able to track the new resonant frequency using the 512-point DFT method described in [6] and adapt the NF frequency to this frequency, thereby producing ripple-free currents. Fig.19 compares the actual resonant frequencies at different L_g values with those detected by the PI and PR control systems. With both producing almost

identical results with the actual values, it is therefore indicative that resonant frequency detection and subsequent control action is independent of controller type and grid strength.

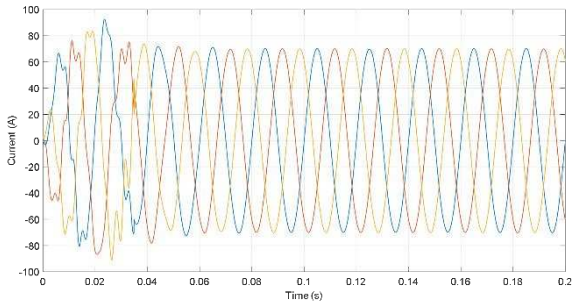

Fig. 17: Grid current under varied grid impedance (PI controller)

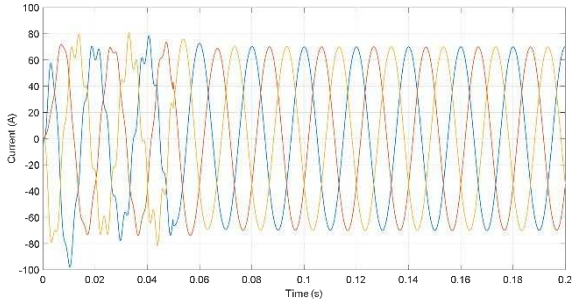

Fig. 18: Grid current under varied grid impedance (PR controller)

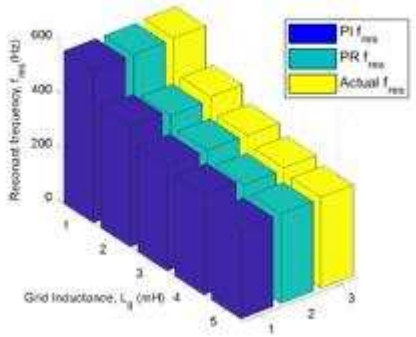

Fig. 19: Bar chart comparing actual resonant frequency to resonant frequency detected by PI and PR control systems

V. CONCLUSION

The paper presents a performance comparison for PI and PR controllers in a grid connected converter with LCL and notch filters. Results indicate that for a weak grid, the PR controller is indeed superior to the PI controller in terms of AC current tracking control and offers higher computational efficiency. In terms of disturbance rejection, the PI controller has shown to be more effective in rejecting DC disturbances that arise in power systems due to faults. With respect to the distorted grid voltage, both controllers are deficient even with the cascaded NF and therefore require additional harmonic compensation techniques. Both control systems, however, are equally efficient with regards to detecting resonant frequency variations due to changes in the grid impedance and subsequently retuning the natural frequency of the cascaded NFs.

REFERENCES

[1] N. B. Lai and K.-H. Kim, "An improved current control strategy for a grid-connected inverter under distorted grid conditions," Energies, vol. 9, no. 3, p. 190, 2016.

[2] R. Teodorescu, F. Blaabjerg, and M. Liserre, "Proportional-resonant controllers. A new breed of controllers suitable for grid-connected voltage-source converters," Proc. Optim, vol. 3, pp. 9-14, 2004.

[3] R. Teodorescu, M. Liserre, and P. Rodriguez, Grid converters for photovoltaic and wind power systems. John Wiley & Sons, 2011.

[4] R. Teodorescu, F. Blaabjerg, M. Liserre, and P. C. Loh, "Proportional-resonant controllers and filters for grid-connected voltage-source converters," IEE Proceedings-Electric Power Applications, vol. 153, no. 5, pp. 750-762, 2006.

[5] M. Cirrincione, M. Pucci, and G. Vitale, Power converters and AC electrical drives with linear neural networks. CRC Press, 2016.

[6] N. A. Rufa'I, L. Zhang, and B. Chong, "Performance analysis of adaptive notch filter active damping methods for grid-connected converters under a varying grid impedance," in PowerTech, 2017 IEEE Manchester, 2017, pp. 1-6: IEEE.

[7] D. Zammit, C. S. Staines, M. Apap, and J. Licari, "Design of PR current control with selective harmonic compensators using Matlab," Journal of Electrical Systems and Information Technology, vol. 4, no. 3, pp. 347-358, 2017.

[8] S. Bacha, I. Munteanu, and A. I. Bratcu, "Power electronic converters modeling and control," Advanced textbooks in control and signal processing, vol. 454, p. 454, 2014.

[9] K. J. Åström and T. Hägglund, PID controllers: theory, design, and tuning. Instrument society of America Research Triangle Park, NC, 1995.

[10] M. Machaba and M. Braae, "Explicit damping factor specification in symmetrical optimum tuning of PI controllers," in Proc. of First African Control Conference, 2003, pp. 3-5.

[11] B. Terzić, G. Majić, and A. Slutej, "Stability analysis of three-phase PWM converter with LCL filter by means of nonlinear model," *AUTOMATIKA: časopis za automatiku, mjerenj*e, elektroniku, *računarstvo i komunikacije,* vol. 51, no. 3, pp. 221-232, 2010.

[12] S. Buso and P. Mattavelli, "Digital control in power electronics," Lectures on power electronics, vol. 1, no. 1, pp. 1-158, 2006.

[13] M. A. Haidekker, Linear feedback controls: the essentials. Newnes, 2013.

[14] J. Huang and X. Yuan, "Impact of the voltage feed-forward and current decoupling on VSC current control stability in weak grid based on complex variables," in Energy Conversion Congress and Exposition (ECCE), 2015 IEEE, 2015, pp. 6845-6852: IEEE.

[15] L. Hewitson, M. Brown, and R. Balakrishnan, Practical power system protection. Elsevier, 2004.

[16] X. Yuan, W. Merk, H. Stemmler, and J. Allmeling, "Stationary-frame generalized integrators for current control of active power filters with zero steady-state error for current harmonics of concern under unbalanced and distorted operating conditions," IEEE transactions on industry applications, vol. 38, no. 2, pp. 523-532, 2002.

[17] P. Kundur, N. J. Balu, and M. G. Lauby, Power system stability and control. McGraw-hill New York, 1994.